Frequency-Dependent Squeezed Vacuum Source for the Advanced Virgo Gravitational-Wave Detector

F. Acernese *et al.*[*]
(Virgo Collaboration)
H. Vahlbruch, M. Mehmet, H. Lück, and K. Danzmann
Institut für Gravitationsphysik, Leibniz Universität Hannover and Max-Planck-Institut für Gravitationsphysik (Albert-Einstein-Institut), Callinstraße 38, 30167 Hannover, Germany[*]

(Received 12 February 2023; revised 24 April 2023; accepted 9 May 2023; published 25 July 2023)

In this Letter, we present the design and performance of the frequency-dependent squeezed vacuum source that will be used for the broadband quantum noise reduction of the Advanced Virgo Plus gravitational-wave detector in the upcoming observation run. The frequency-dependent squeezed field is generated by a phase rotation of a frequency-independent squeezed state through a 285 m long, high-finesse, near-detuned optical resonator. With about 8.5 dB of generated squeezing, up to 5.6 dB of quantum noise suppression has been measured at high frequency while close to the filter cavity resonance frequency, the intracavity losses limit this value to about 2 dB. Frequency-dependent squeezing is produced with a rotation frequency stability of about 6 Hz rms, which is maintained over the long term. The achieved results fulfill the frequency dependent squeezed vacuum source requirements for Advanced Virgo Plus. With the current squeezing source, considering also the estimated squeezing degradation induced by the interferometer, we expect a reduction of the quantum shot noise and radiation pressure noise of up to 4.5 dB and 2 dB, respectively.

DOI: 10.1103/PhysRevLett.131.041403

Introduction.—Interferometric gravitational-wave detectors, such as LIGO and Virgo, have so far observed around 100 gravitational-wave candidate sources, which have already provided several results spanning astrophysics, fundamental physics, and cosmology [1]. These detectors are limited by quantum noise in a large fraction of their operating spectrum. In these modified Michelson interferometers with kilometer-long arms and test masses suspended from pendulums in a cascade, quantum noise manifests itself in two ways: a high-frequency (> 100 Hz) readout noise, so-called shot noise, and a noise that physically displaces the mirrors, the radiation pressure noise (< 100 Hz). The origin of these noises is found in the quantum vacuum fluctuations that enter the detector from the "antisymmetric port," i.e., the point at which the two beams recombine [2]. In a coherent vacuum state, fluctuations of the phase and amplitude (known as coherent quadratures) are equal. However, one can produce, through optical parametric oscillator-based devices, squeezed vacuum states with fluctuations increased on the amplitude quadrature and reduced on the phase quadrature, which also contains the gravitational-wave signal and is effectively detected. [3]. These "squeezed" states were produced and injected into the interferometers during the last (O3) data-taking period (2019-2020). They allowed for a high-frequency sensitivity improvement of 3 dB, which led the detector network to have a significant increase in the number of detected gravitational-wave candidates [4–6]. This "frequency-independent squeezing" (FIS) has the disadvantage, however, of increasing the radiation pressure noise resulting in a potential low-frequency sensitivity degradation as indeed observed by LIGO and Virgo during O3 [7,8]. The reason for this increase is an optomechanically driven and frequency-dependent rotation of the two squeezed vacuum quadratures inside the interferometer, so that at low frequency the gravitational signal is aligned with the quadrature that has larger fluctuations. To reduce the quantum noise in the whole detection bandwidth, a high-finesse optical cavity with suspended mirrors—the "filter cavity" (FC)—can be used to prerotate the produced squeezing quadratures as a function of frequency, allowing the smaller fluctuations quadrature to always be aligned with the gravitational-wave signal [9]. This technique, demonstrated in many prototypes [10–14], has now been developed for Advanced Virgo Plus (AdV+). This article describes the design and performances of the frequency-dependent squeezing (FDS) AdV+ source, before its injection into the interferometer. The source is obtained by combining a

[*]Full author list given at the end of the Letter.

frequency-independent squeezing source and a 285-m, high-finesse Fabry-Perot cavity. Assuming 20% of additional optical losses [15] from the interferometer, the present frequency-dependent squeezing source would make it possible to reduce quantum noise by 4.5 dB at high frequency and 2 dB at low frequency. This represents a relevant improvement in comparison to the FIS configuration used in O3. Considering the impact of other technical noises, this corresponds to an increase in the binary-neutron-star (BNS) and binary-black-hole detection range of up to 9%, with respect to the frequency-dependent squeezing case, which translates into an increase of 29% of the observable-Universe volume. At the same time the 4.5 dB high-frequency noise suppression results in an enhanced sensitivity when searching for higher-frequency sources, such as neutron star late inspirals [16] and postmerger [17] and supernova-core collapses [18].

Experimental setup.—As shown in Fig. 1, the experimental setup is composed of the frequency-independent squeezed vacuum source, which is the same as that used in Virgo during the last observational run (O3) [19] with minor modifications [15], a 285 m long Fabry-Pérot resonator with suspended mirrors, which plays the role of the filter cavity, and two suspended optical benches to inject the squeezed vacuum into the filter cavity and the reflected beam into the interferometer from the antisymmetric port. The system is also equipped with a diagnostic homodyne detector (HD), which is used to characterize the frequency dependent squeezing without needing the interferometer.

Filter cavity: The filter cavity has been designed to have a linewidth of ≈25 Hz, which also corresponds to the desired detuning frequency. Such values have been chosen in order to produce the optimal rotation frequency of the squeezing ellipse, given the interferometer parameters for the forthcoming observing run (O4). Given that some of the squeezing degradation mechanism (e.g., the cavity round-trip losses) are inversely proportional to the cavity length [20], the choice of the cavity extension comes from a trade-off between the reduction of the squeezing degradation due to these effects and the advantage of a smaller infrastructure. The choice of a FC length of 285 m combined with the need of a linewidth of 25 Hz fixes its finesse to $\mathcal{F}_{\mathrm{IR}} \approx 10^4$; experimental measurements gave $\mathcal{F}_{\mathrm{IR}} = 9695 \pm 4$. The other target parameters for the AdV+ FDS source are listed in Table I. A detailed analysis of the reasons that led to the choice of these parameters can be found in Ref. [15].

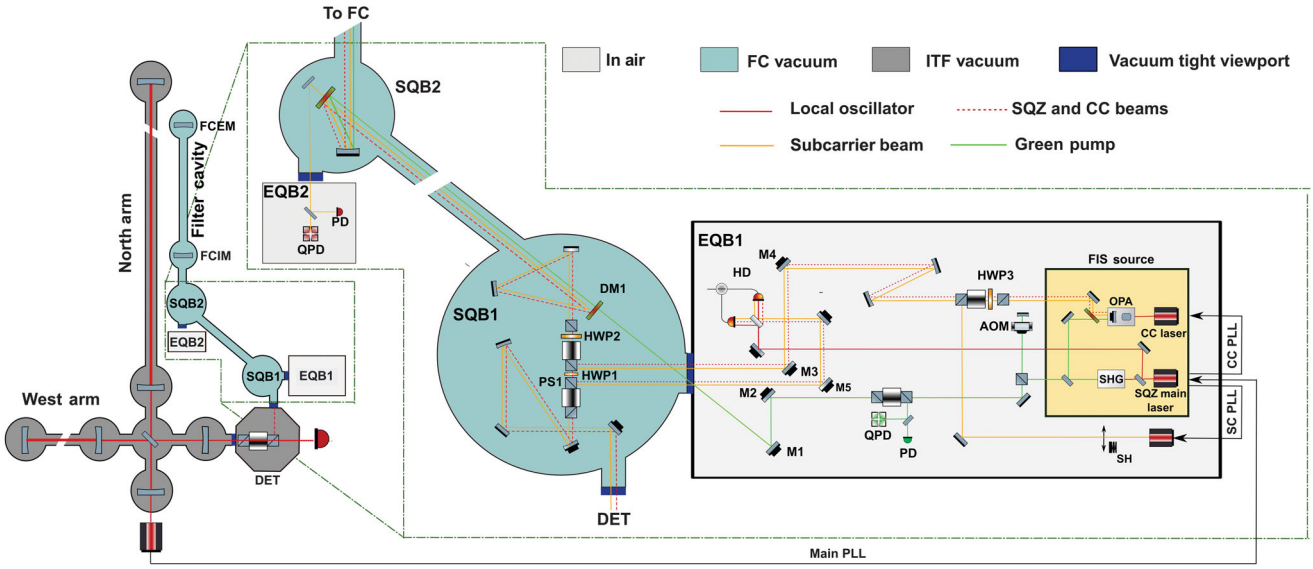

FIG. 1. Experimental setup (not to scale) for the FDS generation installed at the Virgo site. The interferometer arms and the filter cavity are 3 km and 285 m long, respectively, while the SQB1-SQB2 and SQB2-FCIM vacuum tanks are 10 m and 40 m apart, respectively. The expanded area in the green frame contains the simplified optical layout, the description of which can be found in the text. The measurements reported in Figs. 2 and 3 are made with the half-wave plate HWP1, setting the IR beam polarization axis in order to maximize the polarizing beam splitter PS1 reflection toward the M5 mirror, and from there to the diagnostic homodyne detector. Prior to the measurements, the subcarrier beam is used to align the IR fields to the FC. It is subsequently blocked by the motorized shutter SH. This procedure is automatically repeated after each FC unlock. Alternatively, by rotating with HWP1 the beam's polarization by 90°, the IR beams are directed toward the interferometer for squeezing injection, which is part of the currently ongoing second phase of the project. The figure shows the beam paths for the two mutually exclusive cases. The relevant acronyms are as follows: AOM, acousto-optic modulator; HWP, half-wave plate; M, mirror; DM, dichroic mirror; SHG, second harmonic generator; OPA, optical parametric amplifier; HD, homodyne detector; QPD, rf quadrant photodiode; PD, photodiode; PLL, phase locked loop; SH, beam shutter; PS, polarizing beam splitter; DET, detection bench; FCIM and FCEM, filter cavity input and end mirror, respectively.

TABLE I. Measurements and O4 target parameters. The measured injection losses and phase noise parameters do not include the interferometer contribution, which is instead included in the target parameter column.

Degradation parameter	Measured value	O4 design
Injection losses (%)	10 ± 1	13
FC round-trip losses (ppm)	50–90	60
Mode mismatch SQZ-FC (%)	1.5 ± 1	2
Phase noise—rms (mrad)	30 ± 20	40
FC length fluctuation—rms (Hz)	~ 1	1

The cavity is installed inside the Virgo detector's north tunnel, parallel to one of the interferometer arms (see Fig. 1). It comprises two concave mirrors with 150 mm diameter. The radius of curvature (558 m) has been chosen in order to minimize the cavity round-trip losses due to degeneracy with higher order modes [21]. If needed, the radius of curvature can be fine-tuned using ring heaters installed in vacuum around the mirrors [22].

Simulation with measured mirror surface roughness maps shows that this corresponds to a round-trip loss of $\simeq$10 ppm. Scattering from higher-frequency defects has been measured to be 5.5 and 8 ppm for the input [23] and the end [24] mirrors, respectively. The end-mirror transmission is 3.2 ppm, while the coating absorption is below 1 ppm. The expected round-trip losses are therefore less than 30 ppm.

A compact suspension system was designed and implemented for seismic isolation of the filter cavity mirrors. It is composed of a down-scaled version of the Virgo superattenuator inverted pendulum and a geometric antispring filter [25]. The mirrors are then suspended using the standard Virgo "marionette" concept [26].

Auxiliary benches for squeezing injection: The squeezing source is hosted on a nonsuspended in-air optical bench (EQB1) where it is superposed to the auxiliary IR control beams (see below). On the same bench, an acousto-optic modulator is used to set the green beam frequency with respect to the squeezed beam, thus setting the initial detuning condition of the latter.

All these beams are then injected into the vacuum system on the first suspended bench (SQB1). At this level, the IR beams are superposed on the green auxiliary beam, after being reflected by the first polarizer of a double-stage Faraday isolator [27] and they are then sent toward a second suspended bench (SQB2) and to the FC input mirror (see Fig. 1). The IR beams reflected by the FC propagate back to SQB1 together with the green beam where, by selecting the polarization orientation with a half-wave plate (HWP1), it is possible to direct the IR beams either toward the interferometer or toward the diagnostic homodyne detector on EQB1, as in the case of the reported measurements. The green beam propagates back to EQB1, where the sensors for the green control of the FC are located.

In order to achieve the requirements on the residual seismic motion, the in-vacuum benches SQB1 and SQB2 are suspended using a multistage seismic attenuation system [25] that is already used for other auxiliary optical benches in AdV+.

Cavity control strategy: In the configuration used to acquire the FDS measurements reported in this Letter, the FC was longitudinally and angularly controlled with a green (532 nm) beam. This auxiliary field is derived from a pickoff of the optical parametric amplifier (OPA) pump beam, produced by a second harmonic generator (SHG). The finesse of the filter cavity at this wavelength is approximately 100. This corresponds to a much larger bandwidth of the cavity optical resonance for the green, with respect to the IR, which makes the longitudinal control easier to acquire. The error signal for the FC longitudinal control is obtained from the green beam in reflection of the cavity with a Pound-Drever-Hall technique. The correction signals below 100 Hz are sent to the FC end mirror, while the higher-frequency corrections are sent to the laser frequency control. The resulting lock precision, of the order of 1 Hz rms, fulfills the AdV+ design requirement.

The automatic alignment loop that keeps the FC mirrors aligned on the green beam is based on the differential wavefront sensing technique [28] and the correction signal is additionally blended with the optical lever signals at a frequency of 50 mHz. An additional loop, based on the application of a mirror angular position modulation, is used to ensure that the FC optical axis passes through the mirror center.

The squeezing ellipse angle stabilization is obtained via the coherent control technique [29], which requires an auxiliary IR beam with a 4 MHz frequency offset from the squeezed beam.

For the injection of FDS into the interferometer, it is foreseen to control the whole system with IR beams. For this purpose, an auxiliary IR "subcarrier beam" (SC) is added [30]. The SC laser source is phase-locked to the squeezer main laser frequency with a frequency offset $\Omega_{\mathrm{SC}} = 1.262$ GHz. To avoid disturbing the interferometer operation, such offset has been chosen to make the beam antiresonant in the signal recycling cavities and in the output mode cleaner. The SC beam is mode-matched into the OPA and its frequency is also set to be antiresonant for this cavity. As shown in Fig. 1, the beam is thus back-reflected from the OPA and it copropagates with the squeezed field. Misalignment of the SC beam with respect to the filter cavity is sensed by a 0.1% pickoff of the FC reflection, which propagates in the direction of the in-air bench EQB2, where the alignment rf-quadrant photodiodes are hosted. The same bench also hosts the photodiodes for the FC longitudinal control with IR. For the measurements considered in this Letter, the SC beam is only used to prepare the system for the FDS standalone measurement and is subsequently blocked.

Experimental results.—The performance of frequency-dependent squeezed vacuum is highly affected by any optical loss that may occur along the path between the generation of the quantum state inside the OPA and the final measurement at the HD. Therefore, prior to the analyses of FDS measurements and the long-term stability of our setup, an independent loss budget is performed in order to quantify the degradation.

Loss budget: The parameters that degrade the FDS are obtained with independent measurements and are summarized in Table I. The resulting propagation loss between EQB1 to FC, net of the readout losses, is $(10 \pm 1)\%$ and the squeezing ellipse angular noise (31 ± 21) mrad. These parameters have been estimated using the model developed in [31] by comparing squeezing and antisqueezing for various pump powers.

Since the SC beam is 99.8% mode matched to the OPA cavity, it can be used to estimate the mode matching between the squeezed beam and the FC, which is determined to be about 98.5% with long-term fluctuations lower than 1%.

The FC round-trip losses are determined with three different methods [32,33]. The results are distributed over the interval (50–90) ppm, which is higher than the expected value considering only the mirror roughness. The physical origin of this discrepancy has not yet been understood, but it leads to a worsening of the O4 calculated BNS merger horizon of less than 1%.

The readout losses are estimated by taking the measured HD contrast $(98 \pm 1)\%$, the dark noise clearance (1%), and the expected photodiodes quantum efficiency (99%) [19] into account. It is worth noting that, in the case of FDS injection into the interferometer, the readout losses are expected to be different, since a distinct detection system will be used.

Table I summarizes the measured parameters presented in this Letter versus the maximum target values for O4. Except for the FC losses discussed above, the target values have been achieved. Nevertheless, since FDS has not yet been injected into the interferometer, additional contributions from the latter are expected in terms of injection losses and squeezing phase noise.

Frequency-dependent squeezing: In the AdV+ baseline design [15] the bright SC beam is expected to be rejected by the output mode cleaner and can therefore be used for the longitudinal and angular control of the FC without affecting the detection sensitivity. This configuration cannot be used for the squeezing measurements performed with the diagnostic homodyne detector, because the relatively high power of the copropagating SC beam induces saturation and excess technical noise on each homodyne photodiode. Therefore, all of the FDS measurements presented in this Letter are performed with the FC controlled with the green only and the SC beam blocked, relying on the assumption that, during the measurement, the IR alignment and locking to the FC are preserved.

During the commissioning phase of the AdV+ FDS source, several squeezing measurements, with different FC detuning down to a frequency of 25 Hz, have been acquired with the homodyne detector. At frequencies below 20–25 Hz the measurements were often degraded by a non-stationary noise generated by the scattered light produced in the local oscillator (LO) path, which then recombined with the squeezed field [34]. Therefore, the systematic FDS measurements campaign has been done at slightly higher detuning frequencies. It is worth noticing that this detrimental effect is not expected to be relevant when the squeezed field will be injected into the interferometer, since the HD LO will be blocked, while the contribution of the interferometer LO is predicted to be limited, by the Faraday isolators inserted into the squeezed path (see Fig. 1) [15].

A typical set of measurements made at various homodyne angles is shown in Fig. 2, where the level of noise on the HD (in dB) is normalized to the shot noise. The FC detuning $\Delta\omega_{\mathrm{fc}}$ is set at 45 Hz before starting the measurements. The squeezing ellipse angle ϕ_{HD} as seen by the HD is changed by tuning the path length of the LO beam. Using the theoretical model described in [20], the detuning frequency and homodyne angle were fitted, while the loss budget parameters in Table I were kept within the experimental uncertainty ranges. Over time, the fitted detunings, as seen by the squeezed state, show a drift of around 10 Hz, the origin of which is investigated below. At frequencies close to $\Delta\omega_{\mathrm{fc}}$, the squeezing level is degraded by the FC round-trip losses. Nevertheless, even in this frequency range, a shot-noise suppression of at least 2 dB has been observed. At higher frequencies, where the squeezed field is antiresonant to the FC, squeezing levels of down to 5.6 dB are obtained with about 8.5 dB of produced

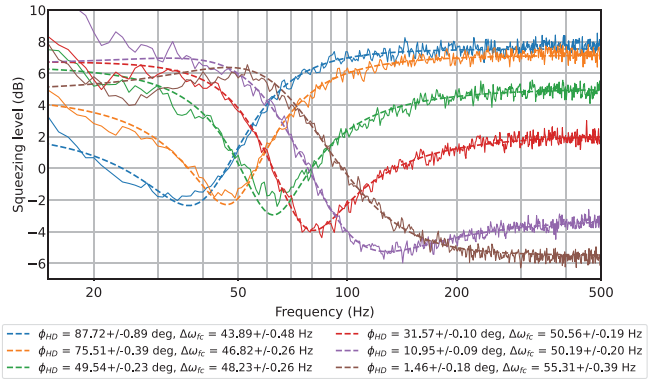

FIG. 2. Relative squeezing level to shot noise in dB (positive is antisqueezing, negative is squeezing) measured at the homodyne detector, for different values of the coherent control phase, and for (44–55) Hz detuning of the FC resonance. The experimental data (solid lines) are fitted using an analytic model of squeezing degradation (dashed lines). The squeezing source generates (8.0–8.5) dB of squeezing. Note that below 20 Hz, all experimental curves increase in noise due to scattered light coupled to low-frequency seismic motion.

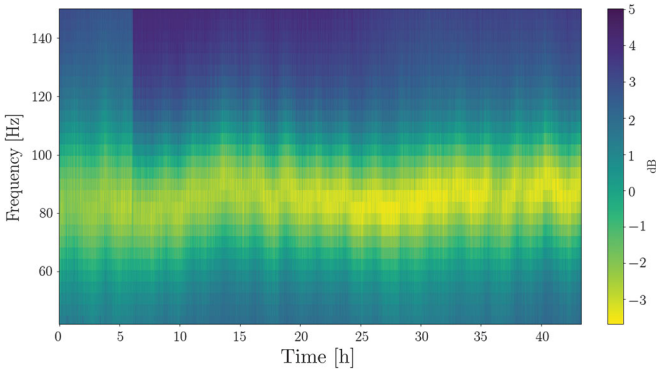

FIG. 3. Power spectral density (PSD) of the diagnostic homodyne detector output normalized to the shot-noise level versus the time of data acquisition. Every 3 min a power spectral density similar to that of Fig. 2 (blue line) with a homodyne angle of 90° is estimated. In correspondence with the acquisition time, the PSD is drawn in the plot with the frequency in the ordinate and the amplitude with a color scale, the calibration of which in dB of squeezing, is represented by the vertical bar on the right. The homodyne angle was chosen to maximize the contrast with which the detuning frequency is observed. The detuning frequency, initially set to be equal to 80 Hz, where the quantum noise suppression is at its maximum, is represented by the yellow curve, which fluctuates in time by about 10 Hz peak to peak. The sudden increase in the antisqueezing level occurring after about 6 h results from an optimization of the infrared alignment.

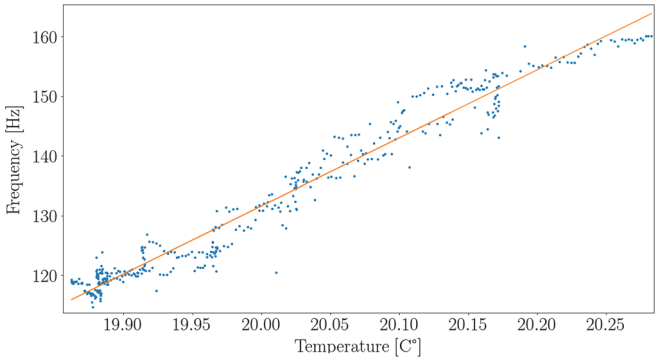

FIG. 4. Filter cavity detuning frequency versus the end mirror ring heater temperature. Each point corresponds to a pair of values measured every 3 min within 24 h. The maximum correlation is obtained assuming that the temperature of the mirror lags behind that of the ring heater by about 60 min.

squeezing. To our knowledge, these results far exceed the reference values obtained in previous publications [13,14] and constitute the state of the art for FDS sources implemented for injection in gravitational-wave interferometric detectors.

Long-term stability: The long-term operation of the FDS system requires additional care in the system controls in order to compensate the daily motion between all of the suspended benches. All these processes, as well as the controls of the squeezing source, are automated in a hierarchical locking procedure managed by a finite state machine [35]. In this way the complete engagement of the FDS measurement after any system failure (for instance a filter cavity unlock) is automatically achieved in less than 4 min.

Figure 3 shows the time frequency plot of the FDS level for a homodyne angle of 90° over a time period of about 48 h. Squeezed light is continuously produced, even if a drift in the squeezing properties is observed. In particular, both the detuning frequency and the squeezing dip amplitude slowly change over time, with an excursion of about 10 Hz and 1 dB, respectively. The antisqueezing value above 1 kHz also changes, reaching a maximum of 8.5 dB with a variation of 1 dB not attributable to variations in the produced antisqueezing level, but rather to the worsening of the infrared alignment to the filter cavity. This behavior is related to the fact that, during the measurement, the FC is fully controlled with the green beam, while the IR fields are not actively locked and aligned to it.

The detuning stability can be affected by several issues when the cavity is operated with a bichromatic control [36], e.g., by the temperature drifts of the cavity mirrors. In fact, the phase acquired after a reflection from the FC mirrors shows a different temperature dependence for green and infrared and this produces IR detuning drifts in the presence of a temperature change when the cavity is locked with the green. This behavior was observed and shown in Fig. 4, reporting a 24-h data acquisition period, in which the temperature of the end mirror was not optimally stabilized. The detuning frequency and the end mirror temperature, approximated by the temperature detected by a thermometer placed on the mirror ring heater, time delayed by 60 min, appear correlated with a scaling factor of (114 ± 1) Hz/K. The slope is in agreement with the results obtained with an analytical model [37]. The applied time lags are justified by the mirror's suspension thermal resistance, which manifests with a time delay in responding to a change in the ring heater temperature. After this observation, the temperature of the mirrors was controlled to better than 30 mK rms, producing the results of Fig. 3.

Although the achieved level of detuning stability would impact less than 1.5% in the best theoretical estimate of the O4 BNS horizon, a lower detuning drift is expected when using the SC-IR beam for filter cavity control. To verify this statement, we locked the OPA to a bright beam derived from the squeezer main laser. Then the OPA output and the SC beams were directed toward the FC and the transmitted IR field was observed while scanning the FC resonance frequency acting on the green acousto-optic modulator. The relative detuning of the two infrared beams, initially set to about 1 kHz, was preserved within 4 Hz over 1 d of acquisition time.

Conclusion.—The frequency-dependent squeezed vacuum source for the broadband quantum noise reduction of the AdV+ detector has been built and characterized at the observatory site. The demonstrated performances in terms of squeezing level and long-term detuning stability

are the best so far reported in the literature. While almost all of the degradation parameters are kept within their designed ranges, the unforeseen value for the FC round-trip loss may reduce the sensitivity for BNS by less than 1%. The actual sensitivity of Advanced Virgo Plus will depend on the squeezing degradation sources and on the residual technical noise of the interferometer. In the design report [15] the interferometer losses were quoted at about 20% [15]. This would produce a high-frequency sensitivity enhancement of about 4.5 dB and with respect to the FIS injection, an increment in the BNS coalescence detection rate of 29%. However, the actual impact of the interferometer losses will be evaluated in the second part of the project, which foresees the injection of the FDS field into the interferometer antisymmetric port.

The authors gratefully acknowledge the support of the Max Planck Society, Leibniz Universität Hannover and Deutsche Forschungsgemeinschaft (DFG, German Research Foundation) through project Grant No. VA 1031/1-1 and Germany's Excellence Strategy—EXC-2123 QuantumFrontiers—390837967 for the construction, installation, and operation of the squeezed light source. The authors gratefully acknowledge the Italian Istituto Nazionale di Fisica Nucleare (INFN), the French Centre National de la Recherche Scientifique (CNRS), and the Netherlands Organization for Scientific Research, for the construction and operation of the Virgo detector and the creation and support of the EGO consortium. The authors also gratefully acknowledge research support from these agencies as well as from the Spanish Agencia Estatal de Investigación, the Consellera d'Innovació, Universitats, Ciència i Societat Digital de la Generalitat Valenciana and the CERCA Programme Generalitat de Catalunya, Spain, the National Science Centre of Poland, the European Commission, the Hungarian Scientific Research Fund (OTKA), the French Lyon Institute of Origins (LIO), the Belgian Fonds de la Recherche Scientifique (FRS-FNRS), Actions de Recherche Concertées (ARC), Fonds Wetenschappelijk Onderzoek—Vlaanderen (FWO), Belgium, École Polytechnique, Japan Society for the Promotion of Science (Grant-in-Aid for Scientific Research No. 21H04476) and the Institute for Cosmic Ray Research (ICRR) and the LabEx UnivEarthS (ANR-10-LABX-0023 and ANR-18-IDEX-0001).

Note added.—At time of writing, FDS sources based on the same operating principle are being commissioned in the two LIGO interferometers, with frequency-dependent squeezing observed at both sites.

[1] LIGO Scientific, the Virgo, the KAGRA Collaborations, GWTC-3: Compact binary coalescences observed by LIGO and Virgo during the second part of the third observing run, arXiv:2111.03606v2.

[2] C. M. Caves, Quantum-mechanical noise in an interferometer, Phys. Rev. D **23**, 1693 (1981).

[3] L. Barsotti, J. Harms, and R. Schnabel, Squeezed vacuum states of light for gravitational wave detectors, Rep. Prog. Phys. **82**, 016905 (2018).

[4] F. Acernese *et al.*, Increasing the Astrophysical Reach of the Advanced Virgo Detector via the Application of Squeezed Vacuum States of Light, Phys. Rev. Lett. **123**, 231108 (2019).

[5] M. Tse *et al.*, Quantum-Enhanced Advanced LIGO Detectors in the Era of Gravitational-Wave Astronomy, Phys. Rev. Lett. **123**, 231107 (2019).

[6] J. Lough, E. Schreiber, F. Bergamin, H. Grote, M. Mehmet *et al.*, First Demonstration of 6 db Quantum Noise Reduction in a Kilometer Scale Gravitational Wave Observatory, Phys. Rev. Lett. **126**, 041102 (2021).

[7] F. Acernese *et al.*, Quantum Backaction on kg-Scale Mirrors: Observation of Radiation Pressure Noise in the Advanced Virgo Detector, Phys. Rev. Lett. **125**, 131101 (2020).

[8] Y. Haocun, L. McCuller1, M. Tse1, N. Kijbunchoo, L. Barsotti, N. Mavalvala *et al.*, Quantum correlations between light and the kilogram-mass mirrors of LIGO, Nature (London) **583**, 43 (2020).

[9] H. J. Kimble, Y. Levin, A. B. Matsko, and K. S. Thorne, Conversion of conventional gravitational-wave interferometers into quantum nondemolition interferometers by modifying their input and/or output optics, Phys. Rev. D **65**, 022002 (2001).

[10] S. Chelkowski, H. Vahlbruch, B. Hage, A. Franzen, N. Lastzka, K. Danzmann, and R. Schnabel, Experimental characterization of frequency-dependent squeezed light, Phys. Rev. A **71**, 013806 (2005).

[11] H. Vahlbruch, S. Chelkowski, B. Hage, A. Franzen, K. Danzmann, and R. Schnabel, Demonstration of a Squeezed-Light-Enhanced Power- and Signal-Recycled Michelson Interferometer, Phys. Rev. Lett. **95**, 211102 (2005).

[12] E. Oelker, T. Isogai, J. Miller, M. Tse, L. Barsotti, N. Mavalvala, and M. Evans, Audio-Band Frequency-Dependent Squeezing for Gravitational-Wave Detectors, Phys. Rev. Lett. **116**, 041102 (2016).

[13] L. McCuller, C. Whittle, D. Ganapathy, K. Komori, M. Tse *et al.*, Frequency-Dependent Squeezing for Advanced LIGO, Phys. Rev. Lett. **124**, 171102 (2020).

[14] Y. Zhao, N. Aritomi, E. Capocasa, M. Leonardi, M. Eisenmann *et al.*, Frequency-Dependent Squeezed Vacuum Source for Broadband Quantum Noise Reduction in Advanced Gravitational-Wave Detectors, Phys. Rev. Lett. **124**, 171101 (2020).

[15] The Virgo Collaboration, Advanced Virgo Plus Phase I—Design Report, Virgo-Technical Documentation System, Report No. VIR-0596A-19, 2019, https://tds.virgo-gw.eu/?content=3&r=15777.

[16] See, for instance, the latest: T. Dietrich, T. Hinderer, and A. Samajdar, Interpreting binary neutron star mergers: Describing the binary neutron star dynamics, modelling gravitational waveforms, and analyzing detections, Gen. Relativ. Gravit. **53**, 27 (2021); Matter imprints in waveform models

for neutron star binaries: Tidal and self-spin effects, Phys. Rev. D **99**, 024029 (2019).
[17] N. Sarin and P. D. Lasky, The evolution of binary neutron star post-merger remnants: A review, Gen. Relativ. Gravit. **53**, 59 (2021).
[18] V. Scrivastava, S. Ballmer, D. A. Brown, C. Afle, A. Burrows, D. Radice, and D. Vartanyan, Detection prospects of core-collapse with supernovae-optimized third generation gravitational-wave detectors, Phys. Rev. D **100**, 043026 (2019).
[19] M. Mehmet and H. Vahlbruch, High-efficiency squeezed light generation for gravitational wave detectors, Classical Quantum Gravity **36**, 015014 (2019).
[20] P. Kwee, J. Miller, T. Isogai, L. Barsotti, and M. Evans, Decoherence and degradation of squeezed states in quantum filter cavities, Phys. Rev. D **90**, 062006 (2014).
[21] E. Capocasa, M. Barsuglia, J. Degallaix, L. Pinard, N. Straniero, R. Schnabel, K. Somiya, Y. Aso, D. Tatsumi, and R. Flaminio, Estimation of losses in a 300m filter cavity and quantum noise reduction in the KAGRA gravitational-wave detector, Phys. Rev. D **93**, 082004 (2016).
[22] I. Nardecchia *et al.*, Optimized radius of curvature tuning for the Virgo core optics, Class. Quantum Grav. **40**, 055004 (2023).
[23] L. Pinard, Input Mirror Characterization Advanced Virgo + Filter Cavity Reference LMA: C20083 + C20087 Virgo-Technical Documentation System, Report No. VIR-1103B-20, 2021, https://tds.virgo-gw.eu/?content=3&r=18118.
[24] L. Pinard, End Mirror Characterization Advanced Virgo + Filter Cavity Reference LMA: C20092 + C20087 Virgo-Technical Documentation System, Report No. VIR-0002A-21, 2021, https://tds.virgo-gw.eu/?content=3&r=18120.
[25] J. V. van Heijningen, A. Bertolini, E. Hennes, M. G. Beker, M. Doets, H. J. Bulten, K. Agatsuma, T. Sekiguchi, and J. F. J. van den Brand, A multistage vibration isolation system for Advanced Virgo suspended optical benches, Classical Quantum Gravity **36**, 075007 (2019).
[26] A. Bernardini *et al.*, Suspension last stages for the mirrors of the Virgo interferometric gravitational wave antenna, Rev. Sci. Instrum. **70**, 3463 (1999).
[27] E. Genin, M. Mantovani, G. Pillant, C. De Rossi, L. Pinard, C. Michel, M. Gosselin, and J. Casanueva, Vacuum-compatible low-loss Faraday isolator for efficient squeezed-light injection in laser-interferometer-based gravitational-wave detectors, Appl. Opt. **57**, 9705 (2018).
[28] N. Mavalvala, Alignment issues in laser interferometric gravitational-wave detectors, Ph.D. thesis, Massachusetts Institute of Technology, 1997.
[29] S. Chelkowski, H. Vahlbruch, K. Danzmann, and R. Schnabel, Coherent control of broadband vacuum squeezing, Phys. Rev. A **75**, 043814 (2007).
[30] Vaishali Badrish Adya, Ways to stop mirrors from moving unnecessarily: Design of advanced gravitational wave detectors, Ph.D. Leibniz University, Hannover, DE, 2018.
[31] E. Schreiber *et al.*, Gravitational-wave detection beyond the quantum shot-noise limit, Ph.D. thesis, Leibniz University Hannover (D), 2018.
[32] E. Capocasa, Y. Guo, M. Eisenmann, Y. Zhao, A. Tomura *et al.*, Measurement of optical losses in a high-finesse 300 m filter cavity for broadband quantum noise reduction in gravitational-wave detectors, Phys. Rev. D **98**, 022010 (2018).
[33] T. Isogai, J. Miller, P. Kwee, L. Barsotti, and M. Evans, Loss in long-storage-time optical cavities, Opt. Express **21**, 30114 (2013).
[34] S. S. Y. Chua *et al.*, Impact of backscattered light in a squeezing enhanced interferometric gravitational-wave detector, Classical Quantum Gravity **31**, 035017 (2014).
[35] F. Carbognani, PYTHON and the Commissioning of the Advanced Virgo Gravitational Waves Detector @ PyCon 08, Virgo-Technical Documentation System, Report No. VIR-0234C-17, 2017, https://tds.virgo-gw.eu/?content=3&r=16343.
[36] Y. Zhao, E. Capocasa, M. Eisenmann, N. Aritomi, M. Page *et al.*, Improving the stability of frequency-dependent squeezing with bichromatic control of filter cavity length, alignment, and incident beam pointing, Phys. Rev. D **105**, 082003 (2022).
[37] M. Lequime, M. Zerrad, and C. Amra, Contribution of HR coatings to the thermal detuning of Virgo filter cavity Virgo-Technical Documentation System, Report No. VIR-0015A-23, 2023, https://tds.virgo-gw.eu/?content=3&r=21455.

F. Acernese,[1,2] M. Agathos,[3] A. Ain,[4] S. Albanesi,[5,6] C. Alléné,[7] A. Allocca,[8,2] A. Amato,[9,10] C. Amra,[11] M. Andia,[12] T. Andrade,[13] N. Andres,[7] M. Andrés-Carcasona,[14] T. Andrić,[15] S. Ansoldi,[16,17] S. Antier,[18] T. Apostolatos,[19] E. Z. Appavuravther,[20,21] M. Arène,[22] N. Arnaud,[12,23] M. Assiduo,[24,25] S. Assis de Souza Melo,[23] P. Astone,[26] F. Aubin,[25] S. Babak,[22] F. Badaracco,[27] S. Bagnasco,[6] J. Baird,[22] T. Baka,[28] G. Ballardin,[23] G. Baltus,[29] B. Banerjee,[15] P. Barneo,[13,30] F. Barone,[31,2] M. Barsuglia,[22] D. Barta,[32] A. Basti,[33,4] M. Bawaj,[34,20] M. Bazzan,[35,36] F. Beirnaert,[37] M. Bejger,[38] V. Benedetto,[39] M. Berbel,[40] S. Bernuzzi,[3] D. Bersanetti,[41] A. Bertolini,[10] U. Bhardwaj,[42,10] A. Bianchi,[10,43] M. Bilicki,[44] S. Bini,[45,46] M. Bischi,[24,25] M. Bitossi,[23,4] M.-A. Bizouard,[18] F. Bobba,[47,48] M. Boër,[18] G. Bogaert,[18] G. Boileau,[49,18] M. Boldrini,[50,26] L. D. Bonavena,[35] R. Bondarescu,[13] F. Bondu,[51] R. Bonnand,[7] V. Boschi,[4] V. Boudart,[29] Y. Bouffanais,[35,36] A. Bozzi,[23] C. Bradaschia,[4] M. Braglia,[52] M. Branchesi,[15,53] M. Breschi,[3] T. Briant,[54] A. Brillet,[18] J. Brooks,[23] G. Bruno,[27] F. Bucci,[25] O. Bulashenko,[13,30] T. Bulik,[55] H. J. Bulten,[10] R. Buscicchio,[56,57] D. Buskulic,[7] C. Buy,[58] G. Cabras,[16,17] R. Cabrita,[27] G. Cagnoli,[59] E. Calloni,[8,2] M. Canepa,[60,41] G. Caneva Santoro,[14] M. Cannavacciuolo,[47] E. Capocasa,[22]

G. Carapella,[47,48] F. Carbognani,[23] M. Carpinelli,[56,61,23] G. Carullo,[33,4] J. Casanueva Diaz,[23] C. Casentini,[62,63] S. Caudill,[10,28] R. Cavalieri,[23] G. Cella,[4] P. Cerdá-Durán,[64] E. Cesarini,[63] W. Chaibi,[18] P. Chanial,[23,22] E. Chassande-Mottin,[22] S. Chaty,[22] P. Chessa,[33,4] F. Chiadini,[65,48] G. Chiarini,[36] R. Chierici,[66] A. Chincarini,[41] M. L. Chiofalo,[33,4] A. Chiummo,[23] N. Christensen,[18] S. Chua,[54] G. Ciani,[35,36] P. Ciecielag,[38] M. Cieślar,[38] M. Cifaldi,[62,63] R. Ciolfi,[67,36] S. Clesse,[68] F. Cleva,[18] E. Coccia,[15,53] E. Codazzo,[15] P.-F. Cohadon,[54] A. Colombo,[56,57] M. Colpi,[56,57] L. Conti,[36] I. Cordero-Carrión,[69] S. Corezzi,[34,20] S. Cortese,[23] J.-P. Coulon,[18] J.-F. Coupechoux,[66] M. Croquette,[54] J. R. Cudell,[29] E. Cuoco,[23,70,4] M. Curyło,[55] P. Dabadie,[59] T. Dal Canton,[12] S. Dall'Osso,[26] G. Dálya,[37] B. D'Angelo,[60,41] G. Dangoisse,[54] S. Danilishin,[9,10] S. D'Antonio,[63] V. Dattilo,[23] M. Davier,[12] J. Degallaix,[71] M. De Laurentis,[8,2] S. Deléglise,[54] F. De Lillo,[27] D. Dell'Aquila,[72,61] W. Del Pozzo,[33,4] F. De Matteis,[62,63] A. Depasse,[27] R. De Pietri,[73,74] R. De Rosa,[8,2] C. De Rossi,[23] R. De Simone,[65] L. Di Fiore,[2] C. Di Giorgio,[47,48] F. Di Giovanni,[64] M. Di Giovanni,[15] T. Di Girolamo,[8,2] D. Diksha,[10,9] A. Di Lieto,[33,4] A. Di Michele,[34] J. Ding,[22,75] S. Di Pace,[50,26] I. Di Palma,[50,26] F. Di Renzo,[23,4] L. D'Onofrio,[8,2] T. Dooney,[28] O. Dorosh,[76] M. Drago,[50,26] J.-G. Ducoin,[77,22] U. Dupletsa,[15] O. Durante,[47,48] D. D'Urso,[72,61] P.-A. Duverne,[12] M. Eisenmann,[78,79] L. Errico,[8,2] D. Estevez,[80] F. Fabrizi,[24,25] F. Faedi,[25] V. Fafone,[62,63,15] G. Favaro,[35] M. Fays,[29] E. Fenyvesi,[32,81] I. Ferrante,[33,4] F. Fidecaro,[33,4] P. Figura,[55] A. Fiori,[4,33] I. Fiori,[23] R. Fittipaldi,[82,48] V. Fiumara,[83,48] R. Flaminio,[7] J. A. Font,[64,84] S. Frasca,[50,26] F. Frasconi,[4] A. Freise,[10,43] O. Freitas,[85] G. G. Fronzé,[6] B. Gadre,[28] R. Gamba,[3] B. Garaventa,[41,60] J. Garcia-Bellido,[52] J. Gargiulo,[23] F. Garufi,[8,2] C. Gasbarra,[62,63] G. Gemme,[41] A. Gennai,[4] Archisman Ghosh,[37] L. Giacoppo,[50,26] P. Giri,[4,33] F. Gissi,[39] S. Gkaitatzis,[23] F. Glotin,[12] B. Goncharov,[15] M. Gosselin,[23] R. Gouaty,[7] A. Grado,[86,2] M. Granata,[71] V. Granata,[47] G. Greco,[20] G. Grignani,[34,20] A. Grimaldi,[45,46] D. Guerra,[64] D. Guetta,[26] G. M. Guidi,[24,25] F. Gulminelli,[87,88] Y. Guo,[10] P. Gupta,[10,28] N. Gutierrez,[71] L. Haegel,[22] O. Halim,[17] O. Hannuksela,[28,10] T. Harder,[18] K. Haris,[10,28] T. Harmark,[89] J. Harms,[15,53] B. Haskell,[38] A. Heidmann,[54] H. Heitmann,[18] P. Hello,[12] G. Hemming,[23] E. Hennes,[10] J.-S. Hennig,[9,10] M. Hennig,[9,10] S. Hild,[9,10] D. Hofman,[71] N. A. Holland,[10,43] V. Hui,[7] G. A. Iandolo,[9] B. Idzkowski,[55] A. Iess,[70,4] G. Iorio,[35] P. Iosif,[90] T. Jacqmin,[54] P.-E. Jacquet,[54] J. Janquart,[28,10] K. Janssens,[49,18] S. Jaraba,[52] P. Jaranowski,[91] P. Jasal,[13] V. Juste,[80] C. Kalaghatgi,[28,10,92] C. Karathanasis,[14] S. Katsanevas,[23] F. Kéfélian,[18] G. Koekoek,[10,9] S. Koley,[15] M. Kolstein,[14] S. L. Kranzhoff,[9,10] A. Królak,[93,76] P. Kuijer,[10] S. Kuroyanagi,[52] P. Lagabbe,[7] D. Laghi,[58] M. Lalleman,[49] A. Lamberts,[18,94] A. La Rana,[26] I. La Rosa,[7] A. Lartaux-Vollard,[12] C. Lazzaro,[35,36] P. Leaci,[50,26] A. Lemaître,[95] M. Lenti,[25,96] E. Leonova,[42] M. Lequime,[11] N. Leroy,[12] N. Letendre,[7] M. Lethuillier,[66] K. Leyde,[22] F. Linde,[92,10] L. London,[42] A. Longo,[97] M. Lopez Portilla,[28] M. Lorenzini,[62,63] V. Loriette,[98] G. Losurdo,[4] D. Lumaca,[62,63] A. Macquet,[14] C. Magazzù,[4] R. Maggiore,[10,43] M. Magnozzi,[41,60] E. Majorana,[50,26] N. Man,[18] V. Mangano,[50,26] M. Mantovani,[23] M. Mapelli,[35,36] F. Marchesoni,[21,20,99] D. Marín Pina,[13,30,100] F. Marion,[7] A. Marquina,[69] S. Marsat,[58] F. Martelli,[24,25] M. Martinez,[14] V. Martinez,[59] A. Masserot,[7] M. Mastrodicasa,[26] S. Mastrogiovanni,[18] Q. Meijer,[28] A. Menendez-Vazquez,[14] L. Mereni,[71] M. Merzougui,[18] A. Miani,[45,46] C. Michel,[71] A. Miller,[27] B. Miller,[42,10] E. Milotti,[101,17] Y. Minenkov,[63] Ll. M. Mir,[14] M. Miravet-Tenés,[64] A. L. Mitchell,[10,43] C. Mondal,[87] M. Montani,[24,25] F. Morawski,[38] G. Morras,[52] A. Moscatello,[35] B. Mours,[80] C. M. Mow-Lowry,[10,43] E. Msihid,[22] F. Muciaccia,[50,26] Suvodip Mukherjee,[42] A. Nagar,[6,102] V. Napolano,[23] I. Nardecchia,[62,63] H. Narola,[28] L. Naticchioni,[26] J. Neilson,[39,48] S. Nesseris,[52] C. Nguyen,[22] G. Nieradka,[38] S. Nissanke,[42,10] E. Nitoglia,[66] F. Nocera,[23] J. Novak,[103,104,105,106] J. F. Nu no Siles,[52] M. Oertel,[103–105,107,106] G. Oganesyan,[15,53] R. Oliveri,[103,104,105] M. Orselli,[20,34] C. Palomba,[26] P. T. H. Pang,[10,28] F. Pannarale,[50,26] F. Paoletti,[4] A. Paoli,[23] A. Paolone,[26,108] G. Pappas,[90] A. Parisi,[4,70] D. Pascucci,[37] A. Pasqualetti,[23] R. Passaquieti,[33,4] D. Passuello,[4] B. Patricelli,[33,4] R. Pedurand,[48] R. Pegna,[4,33] M. Pegoraro,[36] A. Perego,[45,46] A. Pereira,[59] C. Périgois,[67] A. Perreca,[45,46] S. Perriès,[66] J. W. Perry,[10,43] D. Pesios,[90] C. Petrillo,[34] K. S. Phukon,[10,92] O. J. Piccinni,[14] M. Pichot,[18] M. Piendibene,[33,4] F. Piergiovanni,[24,25] L. Pierini,[50,26] G. Pierra,[66] V. Pierro,[39,48] G. Pillant,[23] M. Pillas,[12] F. Pilo,[4] L. Pinard,[71] I. M. Pinto,[39,48,109,8] M. Pinto,[23] M. Pinto,[23] K. Piotrzkowski,[27] A. Placidi,[20,34] E. Placidi,[50,26] W. Plastino,[110,97] R. Poggiani,[33,4] E. Polini,[7] E. Porcelli,[10] J. Portell,[13,30,100] E. K. Porter,[22] R. Poulton,[23] M. Pracchia,[7] T. Pradier,[80] M. Principe,[39,109,48] G. A. Prodi,[111,46] P. Prosposito,[62,63] A. Puecher,[10,28] M. Punturo,[20] F. Puosi,[4,33] P. Puppo,[26] G. Raaijmakers,[42,10] N. Radulesco,[18] P. Rapagnani,[50,26] M. Razzano,[33,4] T. Regimbau,[7] L. Rei,[41] P. Rettegno,[5,6] B. Revenu,[22,112] A. Reza,[10] A. S. Rezaei,[26,50] F. Ricci,[50,26] S. Rinaldi,[33,4] F. Robinet,[12] A. Rocchi,[63] L. Rolland,[7] M. Romanelli,[51] R. Romano,[1,2] A. Romero,[14] S. Ronchini,[15,53] L. Rosa,[2,8] D. Rosińska,[55] S. Roy,[28] D. Rozza,[72,61] P. Ruggi,[23] E. Ruiz Morales,[52] P. Saffarieh,[10,43] O. S. Salafia,[56,57,113] L. Salconi,[23] F. Salemi,[45,46] M. Sallé,[10] A. Samajdar,[57] N. Sanchis-Gual,[114,64] A. Sanuy,[13] A. Sasli,[90] P. Sassi,[20,34] B. Sassolas,[71] S. Sayah,[71] S. Schmidt,[28] M. Seglar-Arroyo,[7] D. Sentenac,[23] V. Sequino,[8,2] G. Servignat,[104] Y. Setyawati,[28] N. S. Shcheblanov,[115,95] M. Sieniawska,[27]

L. Silenzi,[20,21] N. Singh,[55] A. Singha,[9,10] V. Sipala,[72,61] J. Soldateschi,[96,116,25] V. Sordini,[66] F. Sorrentino,[41] N. Sorrentino,[33,4] R. Soulard,[18] V. Spagnuolo,[9,10] M. Spera,[35,36] P. Spinicelli,[23] C. Stachie,[18] D. A. Steer,[22] J. Steinlechner,[9,10] S. Steinlechner,[9,10] N. Stergioulas,[90] G. Stratta,[117,118,26,119] M. Suchenek,[38] A. Sur,[38] J. Suresh,[27] B. L. Swinkels,[10] A. Syx,[80] P. Szewczyk,[55] M. Tacca,[10] N. Tamanini,[58] A. J. Tanasijczuk,[27] E. N. Tapia San Martín,[10] C. Taranto,[62] M. Tonelli,[33,4] A. Torres-Forné,[64] I. Tosta e Melo,[61] E. Tournefier,[7] A. Trapananti,[21,20] F. Travasso,[21,20] J. Trenado,[13] M. C. Tringali,[23] L. Troiano,[120,48] A. Trovato,[17,101] L. Trozzo,[2] K. W. Tsang,[10,121,28] K. Turbang,[122,49] M. Turconi,[18] C. Turski,[37] H. Ubach,[13,30] A. Utina,[9,10] M. Valentini,[45,46] S. Vallero,[6] N. van Bakel,[10] M. van Beuzekom,[10] M. van Dael,[10,123] J. F. J. van den Brand,[9,43,10] C. Van Den Broeck,[28,10] M. van der Sluys,[10,28] A. Van de Walle,[12] J. van Dongen,[10,43] H. van Haevermaet,[49] J. V. van Heijningen,[27] Z. van Ranst,[9] N. van Remortel,[49] M. Vardaro,[92,10] M. Vasúth,[32] G. Vedovato,[36] P. Verdier,[66] D. Verkindt,[7] P. Verma,[76] F. Vetrano,[124] A. Viceré,[24,25] J.-Y. Vinet,[18] S. Viret,[66] A. Virtuoso,[101,17] H. Vocca,[34,20] R. C. Walet,[10] M. Was,[7] N. Yadav,[38] A. Zadrożny,[76] T. Zelenova,[23] J.-P. Zendri,[36] Y. Zhao,[79,125,22] and M. Zerrad[11]

(Virgo Collaboration)

[1]*Dipartimento di Farmacia, Università di Salerno, I-84084 Fisciano, Salerno, Italy*
[2]*INFN, Sezione di Napoli, I-80126 Napoli, Italy*
[3]*Theoretisch-Physikalisches Institut, Friedrich-Schiller-Universität Jena, D-07743 Jena, Germany*
[4]*INFN, Sezione di Pisa, I-56127 Pisa, Italy*
[5]*Dipartimento di Fisica, Università degli Studi di Torino, I-10125 Torino, Italy*
[6]*INFN Sezione di Torino, I-10125 Torino, Italy*
[7]*Université Savoie Mont Blanc, CNRS, Laboratoire d'Annecy de Physique des Particules - IN2P3, F-74000 Annecy, France*
[8]*Università di Napoli "Federico II", I-80126 Napoli, Italy*
[9]*Maastricht University, 6200 MD Maastricht, Netherlands*
[10]*Nikhef, 1098 XG Amsterdam, Netherlands*
[11]*Institut Fresnel, Faculté des Sciences St Jérôme Avenue Escadrille Normandie-Niemen, F-13013 Marseille, France*
[12]*Université Paris-Saclay, CNRS/IN2P3, IJCLab, 91405 Orsay, France*
[13]*Institut de Ciències del Cosmos (ICCUB), Universitat de Barcelona (UB), carrer Martí i Franquès, 1, 08028 Barcelona, Spain*
[14]*Institut de Física d'Altes Energies (IFAE), Barcelona Institute of Science and Technology, and ICREA, E-08193 Barcelona, Spain*
[15]*Gran Sasso Science Institute (GSSI), I-67100 L'Aquila, Italy*
[16]*Dipartimento di Scienze Matematiche, Informatiche e Fisiche, Università di Udine, I-33100 Udine, Italy*
[17]*INFN, Sezione di Trieste, I-34127 Trieste, Italy*
[18]*Université Côte d'Azur, Observatoire Côte d'Azur, CNRS, Artemis, F-06304 Nice, France*
[19]*Department of Physics, National and Kapodistrian University of Athens, 15771 Ilissia, Greece*
[20]*INFN, Sezione di Perugia, I-06123 Perugia, Italy*
[21]*Università di Camerino, I-62032 Camerino, Italy*
[22]*Université Paris Cité, CNRS, Astroparticule et Cosmologie, F-75013 Paris, France*
[23]*European Gravitational Observatory (EGO), I-56021 Cascina, Pisa, Italy*
[24]*Università degli Studi di Urbino "Carlo Bo", I-61029 Urbino, Italy*
[25]*INFN, Sezione di Firenze, I-50019 Sesto Fiorentino, Firenze, Italy*
[26]*INFN, Sezione di Roma, I-00185 Roma, Italy*
[27]*Université catholique de Louvain, B-1348 Louvain-la-Neuve, Belgium*
[28]*Institute for Gravitational and Subatomic Physics (GRASP), Utrecht University, 3584 CC Utrecht, Netherlands*
[29]*Université de Liège, B-4000 Liège, Belgium*
[30]*Departament de Física Quàntica i Astrofísica (FQA), Universitat de Barcelona (UB), carrer Martí i Franqués, 1, 08028 Barcelona, Spain*
[31]*Dipartimento di Medicina, Chirurgia e Odontoiatria "Scuola Medica Salernitana", Università di Salerno, I-84081 Baronissi, Salerno, Italy*
[32]*Wigner RCP, RMKI, H-1121 Budapest, Hungary*
[33]*Università di Pisa, I-56127 Pisa, Italy*
[34]*Università di Perugia, I-06123 Perugia, Italy*
[35]*Università di Padova, Dipartimento di Fisica e Astronomia, I-35131 Padova, Italy*
[36]*INFN, Sezione di Padova, I-35131 Padova, Italy*
[37]*Universiteit Gent, B-9000 Gent, Belgium*
[38]*Nicolaus Copernicus Astronomical Center, Polish Academy of Sciences, 00-716, Warsaw, Poland*
[39]*Dipartimento di Ingegneria, Università del Sannio, I-82100 Benevento, Italy*

[40]Departamento de Matemáticas, Universitat Autònoma de Barcelona, 08193 Bellaterra (Barcelona), Spain
[41]INFN, Sezione di Genova, I-16146 Genova, Italy
[42]GRAPPA, Anton Pannekoek Institute for Astronomy and Institute for High-Energy Physics, University of Amsterdam, 1098 XH Amsterdam, Netherlands
[43]Department of Physics and Astronomy, Vrije Universiteit Amsterdam, 1081 HV Amsterdam, Netherlands
[44]Center for Theoretical Physics, Polish Academy of Sciences, 02-668 Warsaw, Poland
[45]Università di Trento, Dipartimento di Fisica, I-38123 Povo, Trento, Italy
[46]INFN, Trento Institute for Fundamental Physics and Applications, I-38123 Povo, Trento, Italy
[47]Dipartimento di Fisica "E.R. Caianiello", Università di Salerno, I-84084 Fisciano, Salerno, Italy
[48]INFN, Sezione di Napoli, Gruppo Collegato di Salerno, I-80126 Napoli, Italy
[49]Universiteit Antwerpen, 2000 Antwerpen, Belgium
[50]Università di Roma "La Sapienza", I-00185 Roma, Italy
[51]Univ Rennes, CNRS, Institut FOTON - UMR 6082, F-35000 Rennes, France
[52]Instituto de Fisica Teorica UAM-CSIC, Universidad Autonoma de Madrid, 28049 Madrid, Spain
[53]INFN, Laboratori Nazionali del Gran Sasso, I-67100 Assergi, Italy
[54]Laboratoire Kastler Brossel, Sorbonne Université, CNRS, ENS-Université PSL, Collège de France, F-75005 Paris, France
[55]Astronomical Observatory Warsaw University, 00-478 Warsaw, Poland
[56]Università degli Studi di Milano-Bicocca, I-20126 Milano, Italy
[57]INFN, Sezione di Milano-Bicocca, I-20126 Milano, Italy
[58]L2IT, Laboratoire des 2 Infinis - Toulouse, Université de Toulouse, CNRS/IN2P3, UPS, F-31062 Toulouse Cedex 9, France
[59]Université de Lyon, Université Claude Bernard Lyon 1, CNRS, Institut Lumière Matière, F-69622 Villeurbanne, France
[60]Dipartimento di Fisica, Università degli Studi di Genova, I-16146 Genova, Italy
[61]INFN, Laboratori Nazionali del Sud, I-95125 Catania, Italy
[62]Università di Roma Tor Vergata, I-00133 Roma, Italy
[63]INFN, Sezione di Roma Tor Vergata, I-00133 Roma, Italy
[64]Departamento de Astronomía y Astrofísica, Universitat de València, E-46100 Burjassot, València, Spain
[65]Dipartimento di Ingegneria Industriale (DIIN), Università di Salerno, I-84084 Fisciano, Salerno, Italy
[66]Université Lyon, Université Claude Bernard Lyon 1, CNRS, IP2I Lyon / IN2P3, UMR 5822, F-69622 Villeurbanne, France
[67]INAF, Osservatorio Astronomico di Padova, I-35122 Padova, Italy
[68]Université libre de Bruxelles, 1050 Bruxelles, Belgium
[69]Departamento de Matemáticas, Universitat de València, E-46100 Burjassot, València, Spain
[70]Scuola Normale Superiore, I-56126 Pisa, Italy
[71]Université Lyon, Université Claude Bernard Lyon 1, CNRS, Laboratoire des Matériaux Avancés (LMA), IP2I Lyon / IN2P3, UMR 5822, F-69622 Villeurbanne, France
[72]Università degli Studi di Sassari, I-07100 Sassari, Italy
[73]Dipartimento di Scienze Matematiche, Fisiche e Informatiche, Università di Parma, I-43124 Parma, Italy
[74]INFN, Sezione di Milano Bicocca, Gruppo Collegato di Parma, I-43124 Parma, Italy
[75]Corps des Mines, Mines Paris, Université PSL, Paris F-75272, France
[76]National Center for Nuclear Research, 05-400 Świerk-Otwock, Poland
[77]Institut d'Astrophysique de Paris, Sorbonne Université, CNRS, UMR 7095, 75014 Paris, France
[78]Laboratoire dâ Annecy-le-Vieux de Physique des Particules (LAPP), UniversitÂ'e Savoie Mont Blanc, CNRS/IN2P3, F-74941 Annecy-le-Vieux, France
[79]National Astronomical Observatory of Japan, 2-21-1 Osawa, Mitaka, Tokyo 181-8588, Japan
[80]Université de Strasbourg, CNRS, IPHC UMR 7178, F-67000 Strasbourg, France
[81]Institute for Nuclear Research, H-4026 Debrecen, Hungary
[82]CNR-SPIN, I-84084 Fisciano, Salerno, Italy
[83]Scuola di Ingegneria, Università della Basilicata, I-85100 Potenza, Italy
[84]Observatori Astronòmic, Universitat de València, E-46980 Paterna, València, Spain
[85]Centro de Física das Universidades do Minho e do Porto, Universidade do Minho, PT-4710-057 Braga, Portugal
[86]INAF, Osservatorio Astronomico di Capodimonte, I-80131 Napoli, Italy
[87]Université de Normandie, ENSICAEN, UNICAEN, CNRS/IN2P3, LPC Caen, F-14000 Caen, France
[88]Laboratoire de Physique Corpusculaire Caen, 6 boulevard du maréchal Juin, F-14050 Caen, France
[89]Niels Bohr Institute, Copenhagen University, 2100 København, Denmark
[90]Department of Physics, Aristotle University of Thessaloniki, 54124 Thessaloniki, Greece
[91]University of Białystok, 15-424 Białystok, Poland
[92]Institute for High-Energy Physics, University of Amsterdam, 1098 XH Amsterdam, Netherlands
[93]Institute of Mathematics, Polish Academy of Sciences, 00656 Warsaw, Poland
[94]Université Côte d'Azur, Observatoire Côte d'Azur, CNRS, Lagrange, F-06304 Nice, France
[95]NAVIER, École des Ponts, Univ Gustave Eiffel, CNRS, Marne-la-Vallée, France
[96]Università di Firenze, Sesto Fiorentino I-50019, Italy

[97]INFN, Sezione di Roma Tre, I-00146 Roma, Italy
[98]ESPCI, CNRS, F-75005 Paris, France
[99]School of Physics Science and Engineering, Tongji University, Shanghai 200092, China
[100]Institut d'Estudis Espacials de Catalunya, carrer Gran Capità, 2-4, 08034 Barcelona, Spain
[101]Dipartimento di Fisica, Università di Trieste, I-34127 Trieste, Italy
[102]Institut des Hautes Etudes Scientifiques, F-91440 Bures-sur-Yvette, France
[103]Centre national de la recherche scientifique, 75016 Paris, France
[104]Laboratoire Univers et Théories, Observatoire de Paris, 92190 Meudon, France
[105]Observatoire de Paris, 75014 Paris, France
[106]Université PSL, 75006 Paris, France
[107]Université de Paris Cité, 75006 Paris, France
[108]Consiglio Nazionale delle Ricerche - Istituto dei Sistemi Complessi, I-00185 Roma, Italy
[109]Museo Storico della Fisica e Centro Studi e Ricerche "Enrico Fermi", I-00184 Roma, Italy
[110]Dipartimento di Matematica e Fisica, Università degli Studi Roma Tre, I-00146 Roma, Italy
[111]Università di Trento, Dipartimento di Matematica, I-38123 Povo, Trento, Italy
[112]Subatech, CNRS/IN2P3 - Institut Mines-Telecom Atlantique - Université de Nantes,
4 rue Alfred Kastler BP 20722 44307 Nantes C'EDEX 03, France
[113]INAF, Osservatorio Astronomico di Brera sede di Merate, I-23807 Merate, Lecco, Italy
[114]Departamento de Matemática da Universidade de Aveiro and Centre for Research and
Development in Mathematics and Applications, 3810-183 Aveiro, Portugal
[115]Laboratoire MSME, Cité Descartes, 5 Boulevard Descartes, Champs-sur-Marne, 77454 Marne-la-Vallée Cedex 2, France
[116]INAF, Osservatorio Astrofisico di Arcetri, I-50125 Firenze, Italy
[117]Institut für Theoretische Physik, Johann Wolfgang Goethe-Universität, Max-von-Laue-Straße 1, 60438 Frankfurt am Main, Germany
[118]Istituto di Astrofisica e Planetologia Spaziali di Roma, 00133 Roma, Italy
[119]INAF, Osservatorio di Astrofisica e Scienza dello Spazio, I-40129 Bologna, Italy
[120]Dipartimento di Scienze Aziendali - Management and Innovation Systems (DISA-MIS), Università di Salerno,
I-84084 Fisciano, Salerno, Italy
[121]Van Swinderen Institute for Particle Physics and Gravity, University of Groningen, 9747 AG Groningen, Netherlands
[122]Vrije Universiteit Brussel, 1050 Brussel, Belgium
[123]Eindhoven University of Technology, 5600 MB Eindhoven, Netherlands
[124]Università degli Studi di Urbino "Carlo Bo", I-61029 Urbino, Italy
[125]Institute for Cosmic Ray Research (ICRR), KAGRA Observatory, The University of Tokyo,
Kamioka-cho, Hida City, Gifu 506-1205, Japan